Supporting Information on

"Theoretical Study on the Effect of Applying External Static Electric Field on Singlet Fission Dynamics of Pentacene Dimer Models"

Takayoshi Tonami,[1] Ryota Sugimori,[1] Ryota Sakai,[1] Kazuaki Tokuyama,[1] Hajime Miyamoto,[1] Masayoshi Nakano*[1,2,3,4,5]

[1] Department of Materials Engineering Science, Graduate School of Engineering Science, Osaka University, Toyonaka, Osaka 560-8531, Japan

[2] Center for Spintronics Research Network (CSRN), Graduate School of Engineering Science, Osaka University, Toyonaka, Osaka 560-8531, Japan

[3] Center for Quantum Information and Quantum Biology (QIQB), Institute for Open and Transdisciplinary Research Initiatives, Osaka University, Toyonaka, Osaka 560-8531, Japan

[4] Innovative Catalysis Science Division, Institute for Open and Transdisciplinary Research Initiatives, Osaka University, Toyonaka, Osaka 560-8531, Japan

[5] Research Center for Solar Energy Chemistry, Division of Quantum Photochemical Engineering, Graduate School of Engineering Science, Osaka University, Toyonaka, Osaka 560-8531, Japan.

* Corresponding author. E-mail: mnaka@cheng.es.osaka-u.ac.jp

Contents

1. Molecular orbitals for a monomer

In order to clarify the changes in electronic couplings by F, we examine the distributions of the HOMO and LUMO. Fig. S1a shows the distributions of the HOMO-1 – LUMO+1 at F = 0.0 a.u. for one monomer in the tilted-type pentacene dimer model, while Fig. S1b shows the distributions of the density difference of the HOMO and LUMO (ΔHOMO = HOMO(F = 0.005 a.u.) – HOMO(F = 0.0 a.u.) and ΔLUMO = LUMO(F = 0.005 a.u.) – LUMO(F = 0.0 a.u.)) between F = 0.005 and 0.0 a.u. It is found that the distributions of the ΔHOMO and ΔLUMO are similar to those of the LUMO and HOMO, respectively, when F is applied in the x and z directions. Moreover, it is found that the distributions of the ΔHOMO and ΔLUMO are similar to those of the HOMO-1 and LUMO+1, respectively, when F is applied in the y direction. Thus, it turns out that the HOMO under F is described by the linear combination of the HOMO and other frontier MO components, while the LUMO under F is described by that of the LUMO and other frontier MO components.

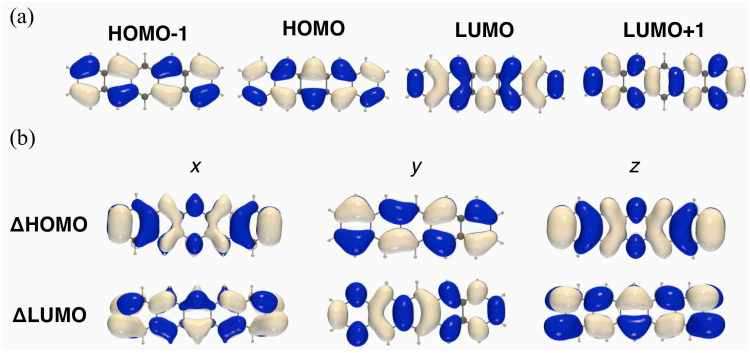

Fig. S1. Distributions of the HOMO-1 – LUMO+1 of pentacene monomer (contour value of ±0.02 a.u.) (a) and the distributions of the density difference of the HOMO(ΔHOMO = HOMO(F = 0.005 a.u.) – HOMO(F = 0.0 a.u.)) and LUMO(ΔLUMO = LUMO(F = 0.005 a.u.) – LUMO(F = 0.0 a.u.)) between F = 0.0 and 0.005 a.u. for a monomer in the tilted-type pentacene dimer model in the case that F is applied in each x, y, and z direction (contour value of ±0.0005 a.u. for the x and z directions and ±0.005 a.u. for the y direction) (b). The white and blue surfaces represent the positive and negative densities with each contour value, respectively.

2. Electronic couplings for the tilted-type pentacene dimer models

We examine the intermolecular orbital interactions for the tilted-type pentacene dimer model at F = 0.0. a.u. Firstly, we analyze the electronic couplings in case that F is applied in the x direction for the tilted-type pentacene dimer model. Since the electronic coupling is related to the intermolecular orbital interaction between monomers, the contribution of intermolecular orbital interaction to each electronic coupling can be approximately described as the summation of the orbital interactions on the facing atom sites between monomers. Therefore, the sign of the electronic coupling is determined by the summation of all the intermolecular orbital interactions on the facing atom sites. Also, the contribution is defined as a negative sign for the intermolecular orbital interaction of the same phase, and as a positive sign for the intermolecular orbital interaction of the opposite phase. Fig. S2a shows the distributions of the HOMO and LUMO on monomer A and B, and Fig. S2b shows those in the middle region (red rectangles in Fig. S2a), where the intermolecular orbital interactions are most likely to contribute to the electronic couplings. For V_{hh} and V_{hl}, it is found that the intermolecular orbital interactions between monomer A and B show the interaction of the same phase because the orbital phases on C atoms facing each other in the zigzag edges of monomers (green rectangles in Fig. S2a and b) are the same, resulting in showing negative V_{hh} and V_{hl} values. In contrast, for V_{lh} and V_{ll}, the intermolecular orbital interactions between monomer A and B are found to show the interaction of the opposite phase because the orbital phases are opposite to each other, resulting in showing positive V_{lh} and V_{ll} values.

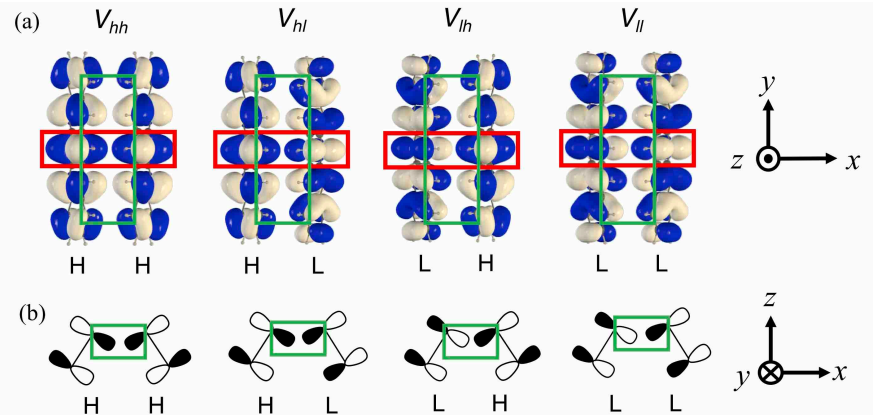

Fig. S2. Distributions of the HOMO (H) and LUMO (L) for the tilted-type pentacene dimer model at $F = 0.0$ a.u. (a), and schematic diagrams of distributions of H and L in the middle region (red rectangles) of the tilted-type pentacene dimer model (b).

Next, we examine the changes of the intermolecular orbital interactions under F. Fig. S3a-c show the distributions of the ΔHOMO and ΔLUMO on monomer A and B by applying F in the x, y, and z directions, respectively. We explain the changes of MOs for the tilted-type pentacene dimer model by applying F in the x directions. Fig. S4a, b, and c show the schematic diagrams of distributions of the HOMO and LUMO at $F = 0.0$ a.u., ΔHOMO and ΔLUMO, and those of the HOMO and LUMO at $F = 0.005$ a.u. on the C atoms facing each other in the zigzag edges of monomers (green rectangles in Fig. S2a and b), respectively. Hereinafter, the HOMO and LUMO at $F = 0.0$ a.u. are referred to as the HOMO and LUMO, respectively, while the HOMO and LUMO at $F = 0.005$ a.u. are referred to as the HOMO' and LUMO', respectively. Because the HOMO' is expressed by HOMO + ΔHOMO, it turns out that the distribution of the HOMO' in the middle of monomer A is decreased (red rectangles in Fig. S4c), while that in the middle of monomer B is increased (green rectangles in Fig. S4c). Similarly, it is found that the distribution of the LUMO' in the middle of monomer A is increased (green rectangles), while that in middle of monomer B is decreased (red rectangles). From these MO distributions, V_{hh} is found to increase because the in-phase interactions between the facing sites in the middle of monomer A and B become weaker by the decrease and increase of the distributions of HOMO' of monomer A and B, respectively. Contrary to V_{hh}, V_{ll} is

found to decrease because the out-of-phase interactions become weaker by the increase and decrease of the distributions of LUMO' of monomer A and B, respectively. Also, it is found that V_{hl} increases because the in-phase interactions of monomer A and B become weaker by the decrease of both the distributions of HOMO' and LUMO' of monomer A and B, respectively. Similarly, it is found that V_{lh} increases because the out-of-phase interactions of monomer A and B become stronger by the increase of both the distributions of the LUMO' and HOMO' of monomer A and B, respectively.

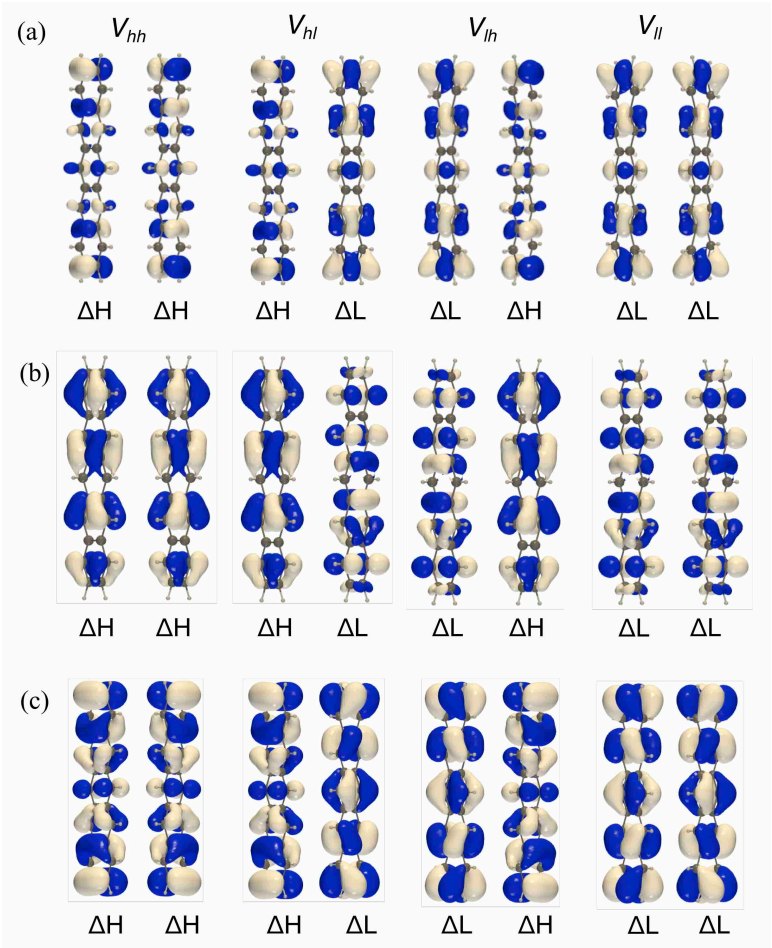

Fig. S3. Distributions (a-c) of the ΔHOMO (ΔH) and ΔLUMO (ΔL) for the tilted-type pentacene dimer model when F = 0.005 a.u. is applied in x, y, and z directions, respectively. White and blue densities represent positive and negative phases, respectively (contour value of ±0.001 a.u. for the x and z directions and ±0.01 a.u. for the y direction).

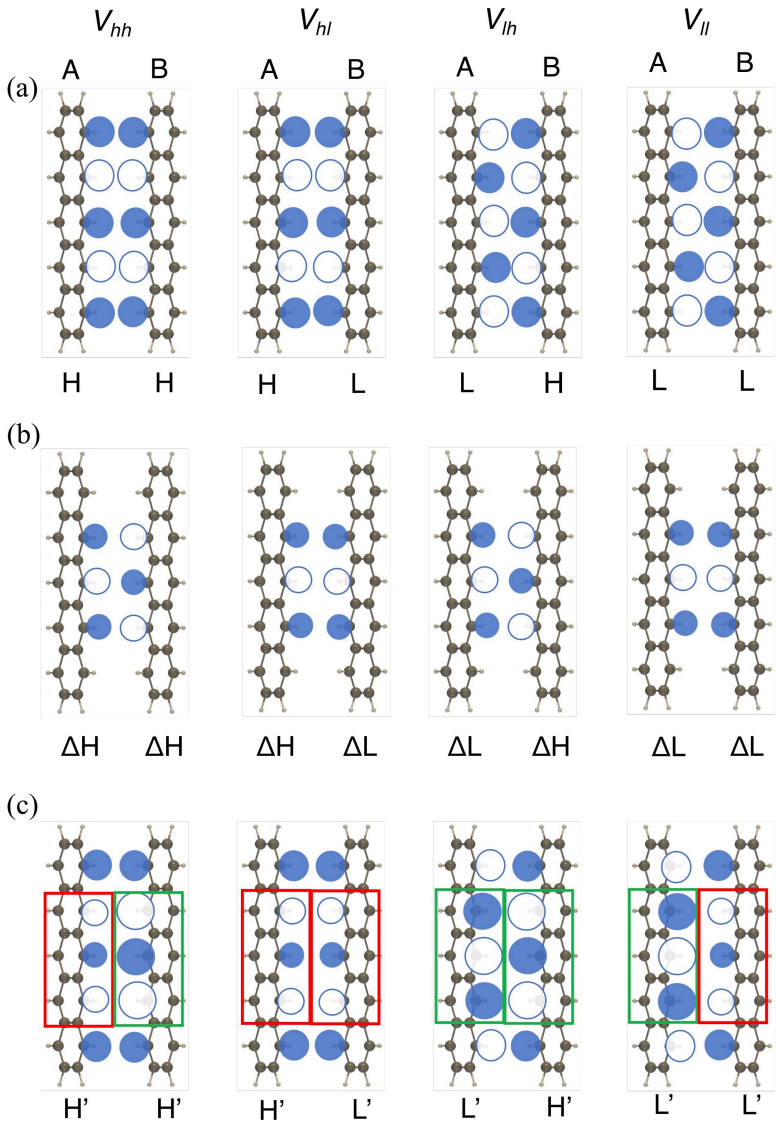

Fig. S4. Schematic diagrams of the distributions of the HOMO (H) and LUMO (L) at F = 0.0 a.u. (a), the ΔHOMO (ΔH) and ΔLUMO (ΔL) (b), and the HOMO (H') and LUMO (L') (c) on the right zigzag edge in monomer A and on the left zigzag edge in monomer B (green rectangles in Fig. S2a and S2b) for the tilted-type pentacene dimer model when F is applied in the x direction. White and blue circles represent positive and negative phases, respectively, and the sizes of circles indicate the relative amplitudes of MOs. Red and green rectangles represent the regions exhibiting relatively smaller and larger amplitudes compared with those at F = 0.0 a.u., respectively.

We examine the changes of MOs for the tilted-type pentacene dimer model by applying F in the y and z directions. Fig. S5a-c show the schematic diagrams of distributions of the HOMO and LUMO, ΔHOMO and ΔLUMO, and the HOMO' and LUMO' on the C atoms facing each other in the zigzag edges of monomers, respectively, when F is applied in the y direction. It turns out that the upper distributions of the HOMO' of monomer A and B are increased (green rectangles in Fig. S5c), while the lower distributions of the HOMO' are decreased (red rectangles in Fig. S5c). Similarly, it is found that the upper distributions of the LUMO' monomer A and B are decreased (red rectangles in Fig. S5c), while that the lower distributions of the LUMO' are increased (green rectangles in Fig. S5c). For V_{hh}, it is found that the in-phase interactions of the upper and lower distributions of HOMOs' become stronger and weaker, respectively. As a result, it is found that V_{hh} is increased on the order of a few meV. Similar to V_{hh}, V_{ll} is found to be increased on the order of a few meV. Also, it is found that V_{hl} increases on the order of a few 10 meV because the in-phase interactions of monomer A and B become weaker by the increase of the upper and lower distributions of HOMO' of A and LUMO' of B, respectively, and the decrease of the lower and upper distributuion of HOMO' of A and LUMO' of B, respectively. Similarly, it is found that V_{lh} is decreased because the out-of-phase interactions between monomer A and B become weaker, respectively.

Fig. S6a-c show the schematic diagrams of distributions of the HOMO and LUMO, ΔHOMO and ΔLUMO, and the HOMO' and LUMO' on the C atoms facing each other in the zigzag edges of monomers, respectively, when F is applied in the z direction. It turns out that the distributions of the HOMO' of monomer A and B are decreased (red rectangles in Fig. S6c), while those of the LUMO' are increased (green rectangles in Fig. S6c). For V_{hh}, it is found that the in-phase interactions between the HOMOs' of monomer A and B become weaker, resulting in the increase of V_{hh}. Contrary to V_{hh}, V_{ll} is found to be increased because the out-of-phase interactions between the LUMOs' of monomer A and B become stronger. Also, V_{hl} is found to decrease because the in-phase interactions become stronger by the decrease and increase of the distributions of HOMO' and LUMO' of monomer A and B, respectively. Similarly, it is found that V_{lh} is increased because the out-of-phase interactions between monomer A and B become stronger by the increase and decrease of the distributions of LUMO' and HOMO' of monomer A and B, respectively.

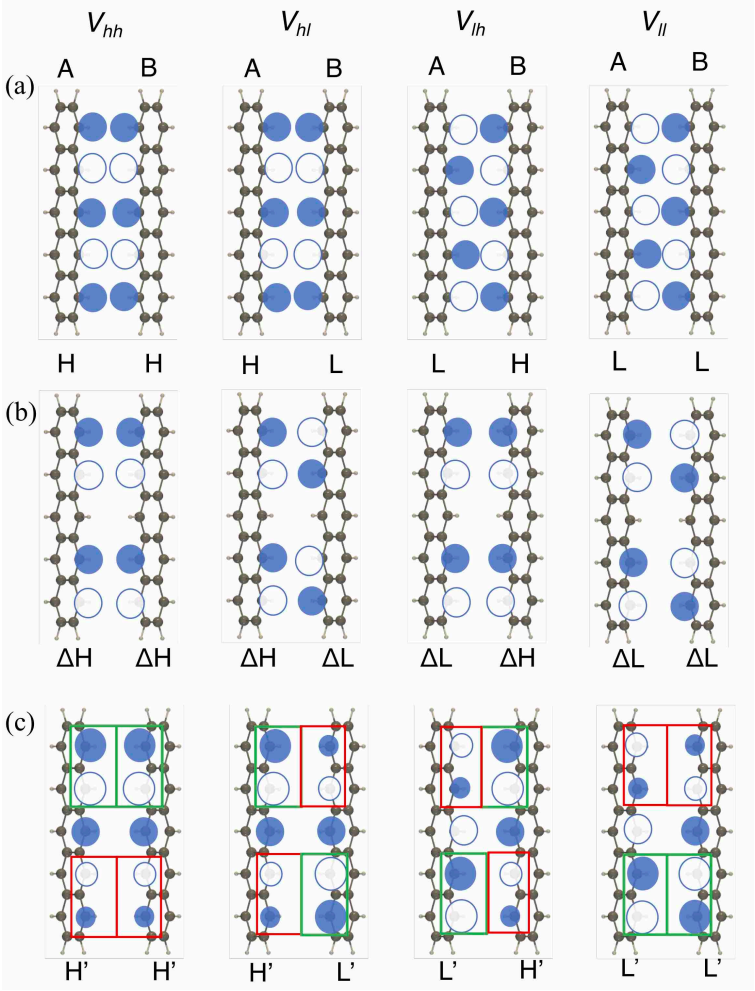

Fig. S5. Schematic diagrams of the distributions of the HOMO (H) and LUMO (L) at F = 0.0 a.u. (a), the ΔHOMO (ΔH) and ΔLUMO (ΔL) (b), and the HOMO (H') and LUMO (L') (c) on the right zigzag edge in monomer A and on the left zigzag edge in monomer B for the tilted-type pentacene dimer model when F = 0.005 a.u. is applied in the y direction. White and blue circles represent positive and negative phases, respectively, and the sizes of circles indicate the relative amplitudes of MOs. Red and green rectangles represent the regions exhibiting relatively smaller and larger amplitudes compared with those at F = 0.0 a.u., respectively.

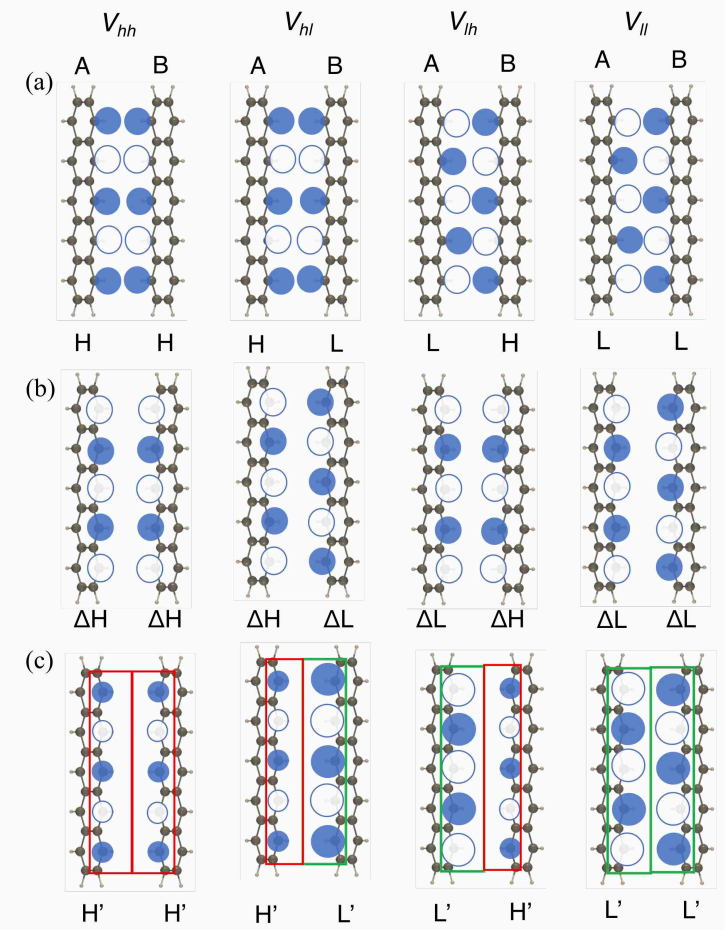

Fig. S6. Schematic diagrams of the distributions of the H and L (a), the ΔH and ΔL (b), and the H' and L' (c) on the right zigzag edge in monomer A and on the left zigzag edge in monomer B for the tilted-type pentacene dimer model when $F = 0.005$ a.u. is applied in the z direction. White and blue circles represent positive and negative phases, respectively, and the sizes of circles indicate the relative amplitudes of MOs. Red and green rectangles represent the regions exhibiting relatively smaller and larger amplitudes compared with those at $F = 0.0$ a.u., respectively.

3. Transition density distribution

It is found that variations of the Frenkel exciton coupling V_{ex} by applying F is significantly small (on the order of 0.01 – 1 meV), which are much smaller than those of the electronic couplings V_{ij}. Fig. S7a shows the transition density distribution between S_1 and S_0 states. Fig. S7b shows the distributions of the transition density differences between F = 0.0 a.u. and 0.005 a.u when F is applied in each x, y, z direction. The changes in the transition density differences cannot been seen unless contour values of these densities are very small (for example, ±0.0001 a.u.).

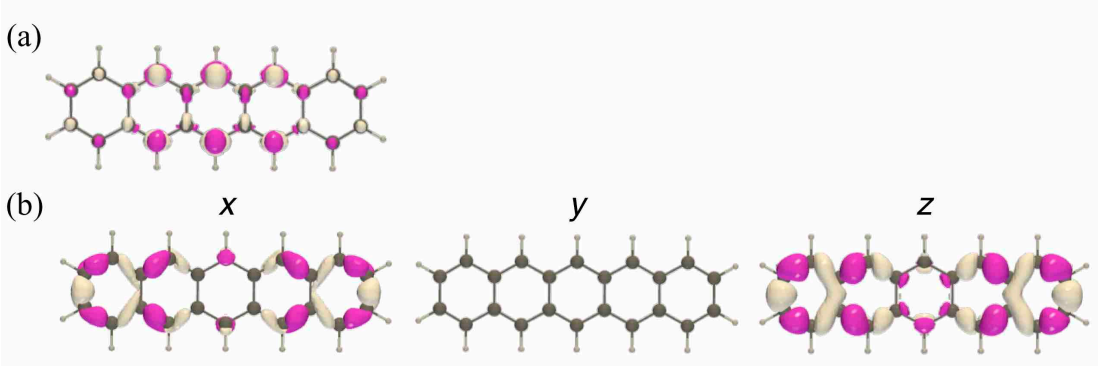

Fig. S7. Distribution of the transition density between S_1 and S_0 states (contour value of ±0.005 a.u.) (a) and the distributions of the transition density differences between F = 0.0 and 0.005 a.u. for a monomer in the tilted-type pentacene dimer model in the case that F is applied in each x, y, and z direction (contour value of ±0.0001 a.u.) (b). The white and magenta surfaces represent the positive and negative densities with each contour value, respectively.

4. Diabatic TT configuration in the lowest adiabatic FE state under the static electric field

We derive the coefficient of the diabatic TT configuration of the adiabatic FE'$_+$ state under F using the first-order perturbation theory in order to clarify the increase of the exciton overlap between FE'$_+$ state and TT' states. We consider the exciton Hamiltonian under F (H_{ex}') using the exciton Hamiltonian at F = 0.0 a.u. (H_{ex}) and the interaction Hamiltonian between the exciton states and F ($H_{ex\text{-}field}$):

$$H_{ex}' = H_{ex} + H_{ex\text{-}field} \tag{s1}$$

Using adiabatic states α of H_{ex}, adiabatic FE'$_+$ state of H_{ex}' (FE''$_+$) is described as follows:

$$\left|\mathrm{FE}''_{+}\right\rangle = \left|\mathrm{FE}'_{+}\right\rangle + \sum_{\alpha(\neq \mathrm{FE}'_{+})} \frac{H_{ex\text{-}field,\alpha\mathrm{FE}'_{+}}}{E(\mathrm{FE}'_{+}) - E(\alpha)} \left|\alpha\right\rangle \tag{s2}$$

Here, $H_{ex\text{-}field,\alpha\mathrm{FE}'_{+}}$ indicates the βFE'$_+$ component of $H_{ex\text{-}field}$ and $E(\alpha)$ represents eigenenergy of the adiabatic states α (α = FE'$_-$, CT'$_+$, CT'$_-$, and TT'). Using diabatic exciton states m, eq s2 is rewritten as follows

$$\begin{aligned}\left|\mathrm{FE}''_{+}\right\rangle &= \left|\mathrm{FE}'_{+}\right\rangle + \sum_{\alpha(\neq \mathrm{FE}'_{+})} \frac{H_{ex\text{-}field,\alpha\mathrm{FE}'_{+}}}{E(\mathrm{FE}'_{+}) - E(\alpha)} \left|\alpha\right\rangle \\ &= \sum_{m} C_{m\mathrm{FE}''_{+}} \left|m\right\rangle\end{aligned} \tag{s3}$$

Here, $C_{m\mathrm{FE}''_{+}}$ indicates the coefficient of the diabatic exciton state m in FE''$_+$ state. Therefore, we prove $C_{\mathrm{TTFE}''_{+}}$ to be non-zero value by applying F. The coefficients of the diabatic TT configuration included in the adiabatic FE'$_+$ and CT'$_+$ states are zero because $V_{lh} + V_{hl} = 0$ is satisfied at F = 0.0 a.u. Therefore, $C_{\mathrm{TTFE}''_{+}}$ is represented by

$$\begin{aligned}C_{\mathrm{TTFE}''_{+}} &= \sum_{\alpha(\neq \mathrm{FE}'_{+})} \frac{H_{ex\text{-}field,\alpha\mathrm{FE}'_{+}}}{E(\mathrm{FE}'_{+}) - E(\alpha)} C_{\mathrm{TT}\alpha} \\ &= \frac{H_{ex\text{-}field,\mathrm{FE}'_{-}\mathrm{FE}'_{+}}}{E(\mathrm{FE}'_{+}) - E(\mathrm{FE}'_{-})} C_{\mathrm{TTFE}'_{-}} + \frac{H_{ex\text{-}field,\mathrm{CT}'_{-}\mathrm{FE}'_{+}}}{E(\mathrm{FE}'_{+}) - E(\mathrm{CT}'_{-})} C_{\mathrm{TTCT}'_{-}} + \frac{H_{ex\text{-}field,\mathrm{TT}'\mathrm{FE}'_{+}}}{E(\mathrm{FE}'_{+}) - E(\mathrm{TT}')} C_{\mathrm{TTTT}'}\end{aligned} \tag{s4}$$

Here, $C_{\mathrm{TTFE'_-}}$, $C_{\mathrm{TTCT'_-}}$, and $C_{\mathrm{TTTT'}}$ indicates the coefficients of the diabatic TT configuration included in the adiabatic FE'–, CT'–, and TT' states at F = 0.0 a.u., respectively. $H_{\text{ex-field}}$ is described by

$$H_{\text{ex-field}} = -\sum_{\alpha,\beta}\mu_{\alpha\beta}F\left|\alpha\right\rangle\left\langle\beta\right| = -\sum_{\alpha,\beta}\sum_{m,n}C_{m\alpha}C_{n\beta}\mu_{mn}F\left|m\right\rangle\left\langle n\right| \tag{s5}$$

Here, μ_{mn} is the *mn* component of the transition dipole moment Hamilonian $\hat{\mu}$, which is described as follows:

$$\hat{\mu} = \begin{array}{c} \begin{matrix} \left|\mathrm{S_1S_0}\right\rangle & \left|\mathrm{S_0S_1}\right\rangle & \left|\mathrm{CA}\right\rangle & \left|\mathrm{AC}\right\rangle & \left|\mathrm{TT}\right\rangle \end{matrix} \\ \begin{pmatrix} 0 & 0 & \mu_{\mathrm{S_1S_0CA}} & \mu_{\mathrm{S_1S_0AC}} & 0 \\ 0 & 0 & \mu_{\mathrm{S_0S_1CA}} & \mu_{\mathrm{S_0S_1AC}} & 0 \\ \mu_{\mathrm{CAS_1S_0}} & \mu_{\mathrm{CAS_0S_1}} & \mu_{\mathrm{CA}} & 0 & \mu_{\mathrm{CATT}} \\ \mu_{\mathrm{ACS_1S_0}} & \mu_{\mathrm{ACS_0S_1}} & 0 & \mu_{\mathrm{AC}} & \mu_{\mathrm{ACTT}} \\ 0 & 0 & \mu_{\mathrm{TTCA}} & \mu_{\mathrm{TTAC}} & 0 \end{pmatrix} \end{array} \tag{s6}$$

Here, because the dipole moment of S_1S_0, S_0S_1, and TT states are zero, diagonal S_1S_0, S_0S_1, and TT components of $\hat{\mu}$ are zero. Also, because $S_1S_0 \rightarrow S_0S_1$, $S_1S_0 \rightarrow$ TT, $S_0S_1 \rightarrow$ TT, and CA → AC transitions involve the two electrons transfer, these transition moments become zero. Therefore, $H_{\text{ex-field,FE'_FE'}_+}$ is described by

$$\begin{aligned} H_{\text{ex-field,FE'_FE'}_+} = -F(&C_{\mathrm{CAFE'_-}}C_{\mathrm{S_1S_0FE'}_+}\mu_{\mathrm{CAS_1S_0}} + C_{\mathrm{ACFE'_-}}C_{\mathrm{S_1S_0FE'}_+}\mu_{\mathrm{ACS_1S_0}} \\ &+ C_{\mathrm{CAFE'_-}}C_{\mathrm{S_0S_1FE'}_+}\mu_{\mathrm{CAS_0S_1}} + C_{\mathrm{ACFE'_-}}C_{\mathrm{S_0S_1FE'}_+}\mu_{\mathrm{ACS_0S_1}} \\ &+ C_{\mathrm{S_1S_0FE'_-}}C_{\mathrm{CAFE'}_+}\mu_{\mathrm{S_1S_0CA}} + C_{\mathrm{S_0S_1FE'_-}}C_{\mathrm{CAFE'}_+}\mu_{\mathrm{S_0S_1CA}} + C_{\mathrm{CAFE'_-}}C_{\mathrm{CAFE'}_+}\mu_{\mathrm{CA}} \\ &+ C_{\mathrm{S_1S_0FE'_-}}C_{\mathrm{CAFE'}_+}\mu_{\mathrm{S_1S_0AC}} + C_{\mathrm{S_0S_1FE'_-}}C_{\mathrm{ACFE'}_+}\mu_{\mathrm{S_0S_1AC}} + C_{\mathrm{ACFE'_-}}C_{\mathrm{ACFE'}_+}\mu_{\mathrm{AC}} \\ &+ C_{\mathrm{TTFE'_-}}C_{\mathrm{CAFE'}_+}\mu_{\mathrm{TTCA}} + C_{\mathrm{TTFE'_-}}C_{\mathrm{ACFE'}_+}\mu_{\mathrm{TTAC}}) \end{aligned} \tag{s7}$$

Moreover, using the HOMO (h_A and h_B) and LUMO (l_A and l_B) of monomer A and B, $\hat{\mu}$ is represented by

$$\hat{\mu}=\begin{pmatrix} 0 & 0 & \mu_{l_A l_B} & -\mu_{h_A h_B} & 0 \\ 0 & 0 & -\mu_{h_A h_B} & \mu_{l_A l_B} & 0 \\ \mu_{l_A l_B} & -\mu_{h_A h_B} & -\mu_{h_A h_A}+\mu_{l_B l_B} & 0 & 2/\sqrt{6}\,\mu_{l_A h_B} \\ -\mu_{h_A h_B} & \mu_{l_A l_B} & 0 & -\mu_{h_B h_B}+\mu_{l_A l_A} & 2/\sqrt{6}\,\mu_{h_A l_B} \\ 0 & 0 & 2/\sqrt{6}\,\mu_{l_A h_B} & 2/\sqrt{6}\,\mu_{h_A l_B} & 0 \end{pmatrix} \quad \text{(s8)}$$

Here, μ_{ij} is described by $\mu_{ij}=-\langle i|\hat{r}|j\rangle$. In the symmetric dimer models, because $C_{\mathrm{CAFE'_-}}=-C_{\mathrm{ACFE'_-}}$, $C_{\mathrm{S_1S_0FE'_+}}=C_{\mathrm{S_0S_1FE'_+}}$, $\mu_{\mathrm{CAS_1S_0}}=\mu_{\mathrm{ACS_0S_1}}$, $\mu_{\mathrm{ACS_1S_0}}=\mu_{\mathrm{CAS_0S_1}}$, $C_{\mathrm{S_1S_0FE'_-}}=-C_{\mathrm{S_0S_1FE'_-}}$, $\mu_{\mathrm{S_1S_0CA}}=\mu_{\mathrm{S_0S_1AC}}$, $\mu_{\mathrm{S_1S_0AC}}=\mu_{\mathrm{S_0S_1CA}}$, and $C_{\mathrm{CAFE'_+}}=C_{\mathrm{ACFE'_+}}$ are satisfied, $H_{\text{ex-field,FE'_FE'_+}}$ is represented by

$$\begin{aligned} H_{\text{ex-field,FE'_FE'_+}} = -F(&C_{\mathrm{CAFE'_-}}C_{\mathrm{CAFE'_+}}\mu_{\mathrm{CA}}+C_{\mathrm{ACFE'_-}}C_{\mathrm{ACFE'_+}}\mu_{\mathrm{AC}} \\ &+C_{\mathrm{TTFE'_-}}C_{\mathrm{CAFE'_+}}\mu_{\mathrm{TTCA}}+C_{\mathrm{TTFE'_-}}C_{\mathrm{ACFE'_+}}\mu_{\mathrm{TTAC}}) \end{aligned} \quad \text{(s9)}$$

Here, the transition moment amplitudes of μ_{TTCA} and μ_{TTAC} are much smaller than the dipole moment amplitudes μ_{CA} and μ_{AC}. Therefore, $H_{\text{ex-field,FE'_FE'_+}}$ is approximately described as follows:

$$H_{\text{ex-field,FE'_FE'_+}} \sim -F(C_{\mathrm{CAFE'_-}}C_{\mathrm{CAFE'_+}}\mu_{\mathrm{CA}}+C_{\mathrm{ACFE'_-}}C_{\mathrm{ACFE'_+}}\mu_{\mathrm{AC}}) \quad \text{(s10)}$$

The same discussion is made for $H_{\text{ex-field,CT'_FE'_+}}$ and $H_{\text{ex-field,TT'FE'_+}}$. Thus, $C_{\mathrm{TTFE''_+}}$ is approximately described by

$$C_{\mathrm{TTFE''_+}} \sim -F\sum_{\substack{\alpha=\mathrm{FE'_-}\\ \mathrm{CT'_-}\\ \mathrm{TT'}}} \frac{C_{\mathrm{CA}\alpha}C_{\mathrm{CAFE'_+}}\mu_{\mathrm{CA}}+C_{\mathrm{AC}\alpha}C_{\mathrm{ACFE'_+}}\mu_{\mathrm{AC}}}{E(\mathrm{FE'_+})-E(\alpha)}C_{\mathrm{TT}\alpha} \quad \text{(s11)}$$

From eq 10, the dipole moments of CA and AC states μ_{CA} and μ_{AC} are found to mainly contribute to the increase of the TT component of FE''$_+$ state by applying *F*.

5. Effect of applying the static electric field on the vibronic coupling

In order to clarify the effect of applying the static electric field on the vibronic coupling, we calculated the reorganization energy λ in S_1 state at the monomer level. λ is given as the summation of the contribution from each normal mode k:

$$\lambda = \sum_k \lambda_k$$
$$\lambda_k = V_k^{\,2} / 2\omega_k \qquad \text{(s12)}$$

Here, λ_k, V_k, and ω_k are the reorganization energy for the normal mode k, the first-order vibronic coupling constant, and the frequency of the normal mode k. V_k is calculated as the gradient of the total energy of S_1 state with respect to nuclear coordinates along the vibrational vector of k at the equilibrium geometry of S_0 state. Fig. S8 shows calculated λ_k values when F = 0.0, 0.001, and 0.005 a.u. is applied in the x direction. The equilibrium geometries of S_0 state, ω_k, and λ_k under F are calculated at the (TD-)RB3LYP/6-311G* level of approximation. It is found that the peaks of (λ_k , ω_k) ~ (48 meV, 175 meV) are obtained at F = 0.0, 0.001, and 0.005 a.u. and trends of λ_k under F are similar to that at F = 0.0 a.u.

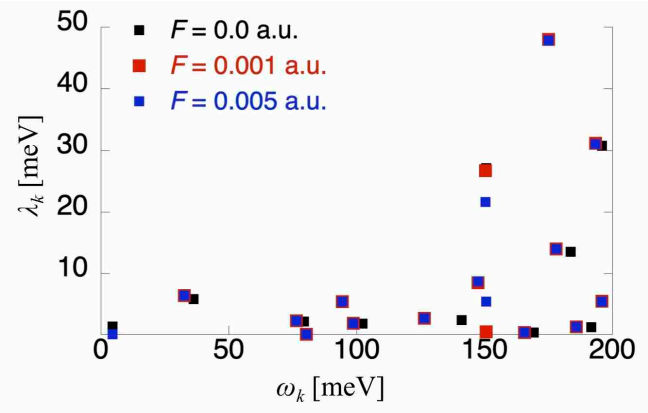

Fig. S8. Reorganization energy λ_k for S_1 state at the monomer level when F = 0.0, 0.001, and 0.005 a.u. is applied in the x direction.

6. Geometries of the tilted- and parallel-type pentacene dimer models

Geometry of the tilted-type pentacene dimer model [Å]

	X	Y	Z
C	0.703139	0.000000	1.217872
C	-0.703139	0.000000	-1.217872
C	0.363883	1.224671	0.630263
C	-0.363883	1.224671	-0.630263
C	0.363883	-1.224671	0.630263
C	-0.363883	-1.224671	-0.630263
H	1.246550	0.000000	2.159088
H	-1.246550	0.000000	-2.159088
C	0.702883	2.464525	1.217429
C	-0.702883	2.464525	-1.217429
C	0.702883	-2.464525	1.217429
C	-0.702883	-2.464525	-1.217429
H	1.246343	2.465162	2.158729
H	-1.246343	2.465162	-2.158729
H	1.246343	-2.465162	2.158729
H	-1.246343	-2.465162	-2.158729
C	0.363494	3.673208	0.629590
C	-0.363494	3.673208	-0.629590
C	0.363494	-3.673208	0.629590
C	-0.363494	-3.673208	-0.629590
C	0.704163	4.935828	1.219646
C	-0.704163	4.935828	-1.219646
C	0.704163	-4.935828	1.219646
C	-0.704163	-4.935828	-1.219646
H	1.247249	4.936896	2.160298
H	-1.247249	4.936896	-2.160298
H	1.247249	-4.936896	2.160298

H	-1.247249	-4.936896	-2.160298
C	0.357919	6.108824	0.619934
C	-0.357919	6.108824	-0.619934
C	0.357919	-6.108824	0.619934
C	-0.357919	-6.108824	-0.619934
H	0.623239	7.055537	1.079481
H	-0.623239	7.055537	-1.079481
H	0.623239	-7.055537	1.079481
H	-0.623239	-7.055537	-1.079481
C	4.203139	0.000000	1.217872
C	5.609416	0.000000	-1.217872
C	4.542395	1.224671	0.630263
C	5.270160	1.224671	-0.630263
C	4.542395	-1.224671	0.630263
C	5.270160	-1.224671	-0.630263
H	3.659727	0.000000	2.159088
H	6.152827	0.000000	-2.159088
C	4.203394	2.464525	1.217429
C	5.609160	2.464525	-1.217429
C	4.203394	-2.464525	1.217429
C	5.609160	-2.464525	-1.217429
H	3.659935	2.465162	2.158729
H	6.152620	2.465162	-2.158729
H	3.659935	-2.465162	2.158729
H	6.152620	-2.465162	-2.158729
C	4.542783	3.673208	0.629590
C	5.269771	3.673208	-0.629590
C	4.542783	-3.673208	0.629590
C	5.269771	-3.673208	-0.629590
C	4.202114	4.935828	1.219646
C	5.610440	4.935828	-1.219646
C	4.202114	-4.935828	1.219646

C	5.610440	-4.935828	-1.219646
H	3.659029	4.936896	2.160298
H	6.153526	4.936896	-2.160298
H	3.659029	-4.936896	2.160298
H	6.153526	-4.936896	-2.160298
C	4.548358	6.108824	0.619934
C	5.264196	6.108824	-0.619934
C	4.548358	-6.108824	0.619934
C	5.264196	-6.108824	-0.619934
H	4.283039	7.055537	1.079481
H	5.529516	7.055537	-1.079481
H	4.283039	-7.055537	1.079481
H	5.529516	-7.055537	-1.079481

Geometry of the parallel-type pentacene dimer model [Å]

	X	Y	Z
C	0.703139	0.000000	1.217872
C	-0.703139	0.000000	-1.217872
C	0.363883	1.224671	0.630263
C	-0.363883	1.224671	-0.630263
C	0.363883	-1.224671	0.630263
C	-0.363883	-1.224671	-0.630263
H	1.246550	0.000000	2.159088
H	-1.246550	0.000000	-2.159088
C	0.702883	2.464525	1.217429
C	-0.702883	2.464525	-1.217429
C	0.702883	-2.464525	1.217429
C	-0.702883	-2.464525	-1.217429
H	1.246343	2.465162	2.158729
H	-1.246343	2.465162	-2.158729
H	1.246343	-2.465162	2.158729

H	-1.246343	-2.465162	-2.158729
C	0.363494	3.673208	0.629590
C	-0.363494	3.673208	-0.629590
C	0.363494	-3.673208	0.629590
C	-0.363494	-3.673208	-0.629590
C	0.704163	4.935828	1.219646
C	-0.704163	4.935828	-1.219646
C	0.704163	-4.935828	1.219646
C	-0.704163	-4.935828	-1.219646
H	1.247249	4.936896	2.160298
H	-1.247249	4.936896	-2.160298
H	1.247249	-4.936896	2.160298
H	-1.247249	-4.936896	-2.160298
C	0.357919	6.108824	0.619934
C	-0.357919	6.108824	-0.619934
C	0.357919	-6.108824	0.619934
C	-0.357919	-6.108824	-0.619934
H	0.623239	7.055537	1.079481
H	-0.623239	7.055537	-1.079481
H	0.623239	-7.055537	1.079481
H	-0.623239	-7.055537	-1.079481
C	4.744590	0.000000	1.217872
C	3.338313	0.000000	-1.217872
C	4.405334	1.224671	0.630263
C	3.677569	1.224671	-0.630263
C	4.405334	-1.224671	0.630263
C	3.677569	-1.224671	-0.630263
H	5.288002	0.000000	2.159088
H	2.794902	0.000000	-2.159088
C	4.744335	2.464525	1.217429
C	3.338569	2.464525	-1.217429
C	4.744335	-2.464525	1.217429

C	3.338569	-2.464525	-1.217429
H	5.287794	2.465162	2.158729
H	2.795109	2.465162	-2.158729
H	5.287794	-2.465162	2.158729
H	2.795109	-2.465162	-2.158729
C	4.404946	3.673208	0.629590
C	3.677958	3.673208	-0.629590
C	4.404946	-3.673208	0.629590
C	3.677958	-3.673208	-0.629590
C	4.745615	4.935828	1.219646
C	3.337289	4.935828	-1.219646
C	4.745615	-4.935828	1.219646
C	3.337289	-4.935828	-1.219646
H	5.288700	4.936896	2.160298
H	2.794203	4.936896	-2.160298
H	5.288700	-4.936896	2.160298
H	2.794203	-4.936896	-2.160298
C	4.399371	6.108824	0.619934
C	3.683533	6.108824	-0.619934
C	4.399371	-6.108824	0.619934
C	3.683533	-6.108824	-0.619934
H	4.664690	7.055537	1.079481
H	3.418213	7.055537	-1.079481
H	4.664690	-7.055537	1.079481
H	3.418213	-7.055537	-1.079481